IEEE Access
Multidisciplinary | Rapid Review | Open Access Journal

Received March 14, 2018, accepted April 9, 2018, date of publication April 24, 2018, date of current version May 24, 2018.

Digital Object Identifier 10.1109/ACCESS.2018.2829839

Hybrid Visual Servo Trajectory Tracking of Wheeled Mobile Robots

FANLEI YAN, BAOQUAN LI, (Member, IEEE), WUXI SHI, AND DONGWEI WANG

Tianjin Key Laboratory of Advanced Technology of Electrical Engineering and Energy, School of Electrical Engineering and Automation, Tianjin Polytechnic University, Tianjin 300387, China

Corresponding author: Baoquan Li (libq@tjpu.edu.cn)

This work was supported in part by the National Natural Science Foundation of China under Grant 61603271 and in part by the Natural Science Foundation of Tianjin under Grant 15JCYBJC47800 and Grant 16JCQNJC03800.

ABSTRACT A hybrid visual trajectory strategy is developed for wheeled mobile robots equipped with onboard vision systems, wherein the 2.5-D visual servoing framework is utilized to enhance trajectory tracking behavior and help to retain visual objects in horizon of the camera. First, according to the current image, the reference image, and the desired images sequence, compound system errors are constructed by both image features and robot orientation. Subsequently, the open-loop error dynamics can be acquired after introducing an error transformation. On this basis, an adaptive controller is developed to achieve the visual servo tracking objective, where the feature depth is compensated online by a parameter updating mechanism. As demonstrated by Lyapunov techniques and Barbalat's Lemma, the proposed visual trajectory tracking controller makes the system errors converge to zero asymptotically in spite of the unknown scene depth. Comparative simulation results are provided to validate the performance of the presented strategy.

INDEX TERMS Visual servoing, wheeled mobile robots, trajectory tracking, Lyapunov technique.

I. INTRODUCTION

With the fast development of robotics technology, wheeled mobile robots are playing an important role nowadays, which are flexible, easy to manipulate, and have large workspace [1]–[3]. In addition, vision sensors have been widely applied to intelligent agents, with advantages such as informative, exteroceptive, and high reliable [4], [5]. After combining mobile robots and vision sensors, it can enhance the ability of external environment perception effectively for the robot system, and then tough missions can be accomplished easily [6]. The vision based control, also termed as visual servoing of mobile robots, utilizes real-time image feedback to steer the mobile robot tracking given trajectories or regulating to target poses. Thus, this technique can be employed extensively in many areas, such as intelligent transportation, home services, and automatic logistics, and becomes one of the most hottest topics in robotics and automation field [7], [8].

Compared with pose regulation control of mobile robots, such as the results in [9], the trajectory tracking scheme can be incorporated with motion planning and multiple system constraints, thus it is more appropriate for implementing complex tasks [10]. For the vision based mobile robot system, one primary challenge is the lack of depth information of the environment, making it difficult to restore the complete pose of the mobile robot and bringing uncertainties for the closed-loop dynamics [11]. On the other hand, the mobile robot is a typical underactuated device having nonholonomic motion constraint [12], thus the existing control methods for robot manipulators, including trajectory tracking such as [13] and [14], cannot be directly applied to mobile robot system. As a result, due to the nonholonomic and even uncertain factors, it is very challenging and equally valuable to design a high-performance visual servo trajectory tracking strategy for wheeled mobile robots.

So far, some methods have been designed to achieve the trajectory tracking objective for mobile robots. Blažič [15] proposes a framework to construct various trajectory tracking controllers, where time-varying functions can be changed to obtain different tracking performance. Based on polar coordinates, Chwa [16] designs a sliding mode controller to track a given trajectory, and the resulting paths present high efficiency and natural behavior. Li *et al.* [17] combine the constrained quadratic programming with model predictive control to solve the trajectory tracking problem, which is constrained by actuator limits of mobile robots. Zambelli *et al.* [18] incorporate tracking errors with descending functions, in order to make it easy to tune the

transient performance in the trajectory tracking process. However, the above tracking methods are valid in the presence that all states of the mobile robot are measurable. So that it brings difficulty for trajectory tracking when utilizing vision sensors, due to the lack of depth information.

When using vision sensors for mobile robot maneuvering, the visual features should be kept in camera field of view [19]. Fang *et al.* [20] utilize pan mechanism to form the active vision, rotating with respect to the visual target. Mariottini and Prattichizzo [21] employ omnidirectional cameras in visual servoing task to keep the features visible when the mobile robot moves. Furthermore, to deal with the unknown depth information, Zhang *et al.* [22] design an adaptive controller in the visual servoing task to compensate the feature depth. While tracking the desired trajectory, Wang *et al.* [23] propose an identification algorithm to provide online estimation of feature depth and robot global position. Yang *et al.* [24] propose an adaptive torque-based trajectory tracking controller for the mobile robot under uncertain robot dynamics and uncalibrated visual parameters. In this sense, the challenges caused by vision sensors, involving the field of view constraint and unknown feature depths, should be disposed very carefully in visual servo tracking tasks.

Many solutions have been developed for visual servo tracking of mobile robots with ceiling cameras [25]. For example, Liang *et al.* [26] propose an image-based trajectory tracking controller with an uncalibrated camera, where the camera plane is not required to be parallel with the robot motion plane. However, the application potentials of the eye-to-hand frame are limited since the mobile robot is restricted in a small area. On the other hand, to accomplish the visual servo tracking tasks of wheeled mobile robots, various methods have been developed for the onboard camera configuration in recent years. Chen *et al.* [27] present a visual trajectory tracking controller with adaptive updating law for the feature depth, where the desired motion trajectories are defined by prerecorded images sequence. To track a given trajectory represented by a series of key images, Jia *et al.* [28] design an adaptive tracking controller to deal with the roughly installed camera. Cherubini and Chaumette [29] utilize key image sequences to define the desired motion path of the mobile robot, and the tracking controller is designed by image errors and obstacle positions. Becerra *et al.* [30] employ epipoles and trifocal tensors to design the angular velocity of the mobile robot, making the system track the given images acquired in large working space. Unfortunately, the existing methods seldom consider the field-of-view problem or investigate the tracking performance.

In this paper, we design a novel visual servo tracking scheme for a wheeled mobile robot carrying an onboard camera. The hybrid visual servoing framework is applied to enhance the trajectory tracking behaviour and make the visual targets easy to be kept in the camera horizon. Firstly, according to the current image, the reference image and the desired images sequence, the 2-1/2-D tracking errors are defined by both image features and robot rotations. Subsequently, an adaptive control law is developed to achieve the visual servo tracking objective, where the feature depth is compensated online by a parameter updating mechanism. According to Lyapunov techniques and LaSalle's invariance principle, the proposed visual servo tracking control law achieves asymptotic stability in spite of unknown scene depth. At last, comparative simulation results are provided to show the performance of the proposed scheme.

In [31], the unified tracking and regulation visual servoing problem is solved, where auxiliary signals are introduced to facilitate the controller design. It is noted that, although this paper borrows some ideas from [31], the controller is redesigned for the specific trajectory tracking task, and then the stability is re-analysed. The proposed scheme has fewer gains to be tuned, and it has good performance for the specific trajectory tracking tasks. Thus, the proposed method is more appropriate for practical using.

The rest of this paper is oulined as follows. Section II formulates the hybrid visual servo tracking task and acquires measurable signals. Section III selects the composite system errors and explores the robot kinematics, then designs the adaptive controller by Lyapunov stability theories. Simulation results are provided in Section IV, and the paper is wrapped up in Section V.

II. SYSTEM MODEL DEVELOPMENT

A. PROBLEM FORMULATION

As shown in Fig. 1, the onboard camera frame $\mathcal{F}^c$ is set coincidentally with that of the nonholonomic mobile robot. The z^c axis of frame $\mathcal{F}^c$ is along the camera optical axis, which is aligned with the front of the mobile robot. The x^c axis is parallel with the wheel axle, and the y^c axis is orthogonal to the robot motion plane $z^c x^c$. Moreover, the desired trajectory, denoted by $\mathcal{F}^d$, is defined by a prerecorded sequence of images with respect to target features through mobile robot movement. The static frame $\mathcal{F}^*$ denotes the reference pose for the robot/camera, which is denoted as the reference frame, enabling the desired and current image sequences can be compared through the constant reference image. Angles $\theta^c(t)$ and $\theta^d(t)$, which can be calculated by homography-based methods, denotes rotation of $\mathcal{F}^c$ and $\mathcal{F}^d$ in regard to the

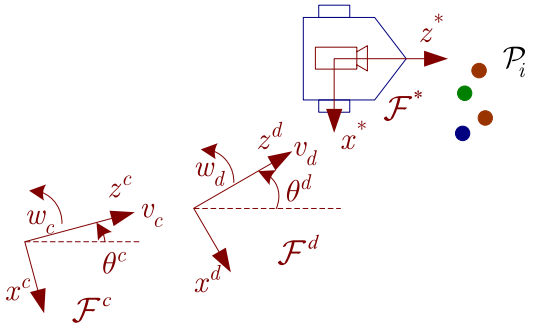

FIGURE 1. Coordinate systems in this visual servoing tracking task.

reference frame, respectively. According to these coordinate systems definition, the objective of the paper is to design a visual servo tracking control law to steer the mobile robot, making $\mathcal{F}^c$ track trajectories defined by the frame $\mathcal{F}^d$.

It is noted that, for practical use, any of the image in the desired image sequence can be used as the reference image. Thus, the reference image does not need to be captured any more after recording the desired image sequence.

B. MEASURABLE SIGNALS

Consider N static feature points $\mathcal{P}_i (i = 1, 2, \ldots, N)$ in the scene, with $\boldsymbol{P}_i^*, \boldsymbol{P}_i^d, \boldsymbol{P}_i^c \in \mathbb{R}^3$ being the 3-D Euclidean coordinates described in the frames $\mathcal{F}^*$, $\mathcal{F}^d$ and $\mathcal{F}^c$, respectively, as follows:

$$\boldsymbol{P}_i^* = \begin{bmatrix} X_i^* \\ Y_i^* \\ Z_i^* \end{bmatrix}, \quad \boldsymbol{P}_i^d = \begin{bmatrix} X_i^d \\ Y_i^d \\ Z_i^d \end{bmatrix}, \quad \boldsymbol{P}_i^c = \begin{bmatrix} X_i^c \\ Y_i^c \\ Z_i^c \end{bmatrix}. \tag{1}$$

The corresponding homogeneous image pixel coordinates $\boldsymbol{p}_i^*, \boldsymbol{p}_i^d, \boldsymbol{p}_i^c \in \mathbb{R}^3$ are expressed as

$$\boldsymbol{p}_i^* = \begin{bmatrix} u_i^* \\ v_i^* \\ 1 \end{bmatrix}, \quad \boldsymbol{p}_i^d = \begin{bmatrix} u_i^d \\ v_i^d \\ 1 \end{bmatrix}, \quad \boldsymbol{p}_i^c = \begin{bmatrix} u_i^c \\ v_i^c \\ 1 \end{bmatrix}. \tag{2}$$

According to [32], the normalized image coordinates are measurable by

$$\begin{aligned} \bar{\boldsymbol{p}}_i^* &= K^{-1}\boldsymbol{p}_i^* = \begin{bmatrix} x_i^* & y_i^* & 1 \end{bmatrix}^T, \\ \bar{\boldsymbol{p}}_i^d &= K^{-1}\boldsymbol{p}_i^d = \begin{bmatrix} x_i^d & y_i^d & 1 \end{bmatrix}^T, \\ \bar{\boldsymbol{p}}_i^c &= K^{-1}\boldsymbol{p}_i^c = \begin{bmatrix} x_i^c & y_i^c & 1 \end{bmatrix}^T \end{aligned} \tag{3}$$

where $K \in \mathbb{R}^{3\times 3}$ is the known camera intrinsic matrix.

To facilitate the subsequent analysis, the depth ratios are defined as follows:

$$\gamma_{i1} := \frac{Z_i^*}{Z_i^d}, \quad \gamma_{i2} := \frac{Z_i^*}{Z_i^c}. \tag{4}$$

The variables $Z_i^d(t)$ and $Z_i^c(t)$ are positive since the mobile robot keeps a certain distance from the object target generally. Hence, there will be no singularity for $\gamma_{i1}(t)$ and $\gamma_{i2}(t)$, which can be estimated by $\gamma_{i1} = y_i^d/y_i^*$, $\gamma_{i2} = y_i^c/y_i^*$.

From [31], it is known that the desired angular velocity $w_d(t)$ and the scaled desired linear velocity $\bar{v}_d := (Z_i^*)^{-1} v_d$ can be estimated by the following differential algorithm:

$$\begin{aligned} w_d &= \frac{\theta^d(k) - \theta^d(k-1)}{\Delta t_k} \\ \bar{v}_d &= \frac{1}{\Delta t_k}\left(\frac{y_i^d(k)}{y_i^d(k-1)} - 1\right)\gamma_{i1}^{-1} - \gamma_{i1}^{-1} x_i^d w_d \end{aligned} \tag{5}$$

where $\theta^d(k)$ is the value of $\theta^d(t)$ at current time, $\theta^d(k-1)$ denotes for the value of $\theta^d(t)$ at the previous time instant, same to $y_i^d(k)$ and $y_i^d(k-1)$, and Δt_k is the interval between the two time instants.

III. CONTROL DEVELOPMENT

In this section, the robot kinematics is analyzed at first, then the trajectory tracking controller is designed with actively compensating for the unknown feature depth, and Lyapunov techniques are employed to demonstrate that the proposed controller can make the tracking errors converge to zero asymptotically.

A. ROBOT KINEMATICS

The translation errors $e_z(t)$, $e_x(t)$ between $\mathcal{F}^c$ and $\mathcal{F}^d$, which can be written by any feature point $\mathcal{P}_i$, are defined without any singularity as follows:

$$\begin{bmatrix} e_z \\ e_x \end{bmatrix} := \frac{1}{Z_i^*}\begin{bmatrix} \cos\theta^d & -\sin\theta^d \\ \sin\theta^d & \cos\theta^d \end{bmatrix}\begin{bmatrix} Z_i^c \\ X_i^c \end{bmatrix} - \frac{1}{Z_i^*}\begin{bmatrix} \cos\theta^c & -\sin\theta^c \\ \sin\theta^c & \cos\theta^c \end{bmatrix}\begin{bmatrix} Z_i^d \\ X_i^d \end{bmatrix} \tag{6}$$

Morevoer, the orientation error $e_\theta(t)$ between $\mathcal{F}^c$ and $\mathcal{F}^d$ is defined as

$$e_\theta := \theta^c - \theta^d. \tag{7}$$

So we know that the tracking errors are constructed by both image features and the calculated orientation angles, making the designed scheme belong to the category of 2.5D visual servoing frame, which helps to keep the visual target in camera horizon.

To facilitate control development in next part, a new error vector is designed as

$$\begin{bmatrix} \rho_1 \\ \rho_2 \\ \rho_3 \end{bmatrix} := \begin{bmatrix} 1 & 0 & 0 \\ 0 & \cos\theta^d & \sin\theta^d \\ 0 & -\sin\theta^d & \cos\theta^d \end{bmatrix}\begin{bmatrix} e_\theta \\ e_z \\ e_x \end{bmatrix}. \tag{8}$$

After taking the time derivative of $\rho_1(t)$, $\rho_2(t)$ and $\rho_3(t)$, the chained-form system kinematics can be obtained as follows [31]:

$$\begin{cases} \dot{\rho}_1 = w_c - w_d, \\ \dot{\rho}_2 = -\alpha^{-1} v_c + \bar{v}_d \cos\rho_1 - \rho_3 w_c, \\ \dot{\rho}_3 = \bar{v}_d \sin\rho_1 + \rho_2 w_c \end{cases} \tag{9}$$

where the unknown depth information is denoted as $\alpha := Z_i^*$. Moreover, the error signals $e_z(t)$, $e_x(t)$, $e_\theta(t)$ can be obtained after utilizing the homography-based algorithms, and the overall hybrid tracking system is shown in Fig. 2. Since the control framework has been re-designed with respect to the specific trajectory tracking task, we see that this figure is different with [31, Fig. 2].

To facilitate the control design in the next part, we make the following assumption.

Assumption 1: The desired velocities $v_d(t), w_d(t)$ are bounded for all time and that $\lim_{t\to\infty} v_d(t) \neq 0$.

B. CONTROLLER DESIGN

On the basis of the open-loop error system in (9), an adaptive visual servoing controller is developed for the wheeled

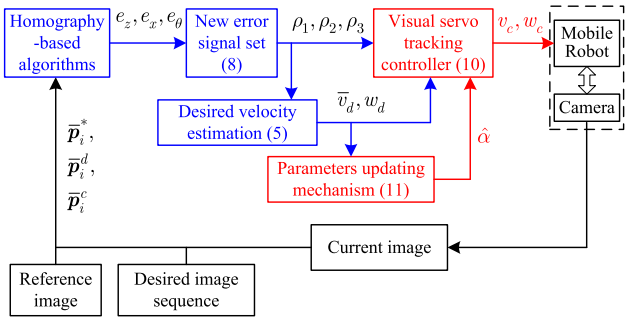

FIGURE 2. Block diagram for the overall hybrid tracking system.

mobile robot in this part, despite the feature depth is unknown.

According to the Lyapunov-based controller design methods, the linear and angular velocities of the mobile robot are designed as follows:

$$\begin{aligned} v_c &= k_v\rho_2 + \rho_3 w_c + \hat{\alpha}(\bar{v}_d\cos\rho_1 - \rho_3 w_c),\\ w_c &= -k_w\rho_1 + \frac{\sin\rho_1}{\rho_1}\rho_3\bar{v}_d + w_d \end{aligned} \tag{10}$$

where k_v, k_w are positive control gains. $\hat{\alpha}$ is the estimate of the constant α relating to the unknown depth, and it is updated by the following mechanism:

$$\dot{\hat{\alpha}} = \Gamma\rho_2(\bar{v}_d\cos\rho_1 - \rho_3 w_c) \tag{11}$$

where $\Gamma \in \mathbb{R}^+$ is the update gain.

After substituting the designed controller into the open-loop dynamics (9), the closed-loop system is obtained as follows:

$$\begin{cases} \dot{\rho}_1 = -k_w\rho_1 + \dfrac{\sin\rho_1}{\rho_1}\rho_3\bar{v}_d,\\ \alpha\dot{\rho}_2 = -k_v\rho_2 - \rho_3 w_c + \tilde{\alpha}(\bar{v}_d\cos\rho_1 - \rho_3 w_c),\\ \dot{\rho}_3 = \bar{v}_d\sin\rho_1 + \rho_2 w_c \end{cases} \tag{12}$$

where $\tilde{\alpha}$ defines the parameter estimation error as $\tilde{\alpha} := \alpha - \hat{\alpha}$.

Theorem 1: The control law (10), together with the parameter updating mechanism (11), enable the errors of the system dynamic (9) go to zero in the sense that

$$\lim_{t\to\infty} e_z(t), e_x(t), e_\theta(t) = 0.^1 \tag{13}$$

Proof: The nonnegative Lyapunov function candidate $V(t)$ is chosen as follows:

$$V = \frac{1}{2}\rho_1^2 + \frac{1}{2}\alpha\rho_2^2 + \frac{1}{2}\rho_3^2 + \frac{1}{2}\Gamma^{-1}\tilde{\alpha}^2 \tag{14}$$

After taking the derivative of both sides of (14) and then using the closed-loop dynamics (12), we know that

$$\dot{V} = -k_w\rho_1^2 - k_v\rho_2^2 + \rho_2\tilde{\alpha}(\bar{v}_d\cos\rho_1 - \rho_3 w_c) - \Gamma^{-1}\tilde{\alpha}\dot{\hat{\alpha}} \tag{15}$$

[1]From (6) and (7), it is known that when formula (13) holds, the visual servo tracking task is achieved.

After substituting (11) into (15), the following formula is obtained:

$$\dot{V} = -k_w\rho_1^2 - k_v\rho_2^2. \tag{16}$$

Using (14) and (16), it is easy to know that $\rho_1(t)$, $\rho_2(t)$, $\rho_3(t)$, $\tilde{\alpha}(t) \in \mathcal{L}_\infty$. Then, from (10) we have $v_c(t)$, $w_c(t) \in \mathcal{L}_\infty$, with the assumption $v_d(t)$, $w_d(t)$ are bounded. Hence, based on (9) and (11), it is obtained that $\dot{\rho}_1$, $\dot{\rho}_2$, $\dot{\rho}_3$, $\dot{\tilde{\alpha}}$, $\in \mathcal{L}_\infty$. Therefore, the evolution of all system states are kept bounded.

Moreover, from (16) it is known that ρ_1, $\rho_2 \in \mathcal{L}_2$. Thus, the Barbalat's Lemma can be directly used to obtain that $\lim_{t\to\infty} \rho_1(t), \rho_2(t) = 0$.

Then, we take the derivative of the entity $\sin\rho_1/\rho_1$ in the dynamics of $\rho_1(t)$ in (12) as follows:

$$\frac{\mathrm{d}}{\mathrm{d}\rho_1}\left(\frac{\sin\rho_1}{\rho_1}\right) = \frac{\rho_1\cos\rho_1 - \sin\rho_1}{\rho_1^2} \tag{17}$$

and the following relationships hold:

$$\lim_{\rho_1\to\infty}\frac{\rho_1\cos\rho_1 - \sin\rho_1}{\rho_1^2} = 0, \tag{18}$$

$$\begin{aligned} \lim_{\rho_1\to 0}\frac{\rho_1\cos\rho_1 - \sin\rho_1}{\rho_1^2} &= \lim_{\rho_1\to 0}\frac{\cos\rho_1 - \rho_1\sin\rho_1 - \cos\rho_1}{2\rho_1}\\ &= \lim_{\rho_1\to 0}\frac{-\rho_1\sin\rho_1}{2\rho_1} = 0 \end{aligned} \tag{19}$$

and it is known that $(\rho_1\cos\rho_1 - \sin\rho_1)/\rho_1^2$ is continuous in the interval $(0, \infty)$. Thus, it can be concluded that $(\rho_1\cos\rho_1 - \sin\rho_1)/\rho_1^2 \in \mathcal{L}_\infty$. Then it is seen that $\sin\rho_1/\rho_1$ is uniformly continuous.

Furthermore, it is easy to obtain that $(\sin\rho_1/\rho_1)\rho_3\bar{v}_c^d$ is also uniformly continuous. We also have $\lim_{t\to\infty} k_w\rho_1 = 0$ and $\lim_{t\to\infty}\rho_1 =$ constant. Hence, the Extended Barbalat's Lemma [2] can be employed on the dynamics of $\rho_1(t)$ in (12) to prove that

$$\lim_{t\to\infty}\frac{\sin\rho_1}{\rho_1}\rho_3\bar{v}_c^d = 0. \tag{20}$$

Because of the assumption $\lim_{t\to\infty} v_d(t) \neq 0$, it is easy to see $\lim_{t\to\infty}\rho_3(t) = 0$.

Therefore, we know that all the system states converge to the origin asymptotically, namely $\lim_{t\to\infty}\rho_1(t)$, $\rho_2(t)$, $\rho_3(t) = 0$.

Furthermore, based on the relationship between $\rho_1(t)$, $\rho_2(t)$, $\rho_3(t)$ and $e_z(t)$, $e_x(t)$, $e_\theta(t)$ in (8), the trajectory tracking errors converge to zero asymptotically, that is $\lim_{t\to\infty} e_z(t), e_x(t), e_\theta(t) = 0$. □

IV. SIMULATION RESULTS

The simulation tests are provided in this section to validate the performance of this designed scheme. In the simulation, 4 randomly selected co-planar feature points are taken as visual targets, and the reference image is acquired at $\mathcal{F}^*$. To obtain the desired images sequence, which defines the desired robot motion trajectory, the virtual robot-camera

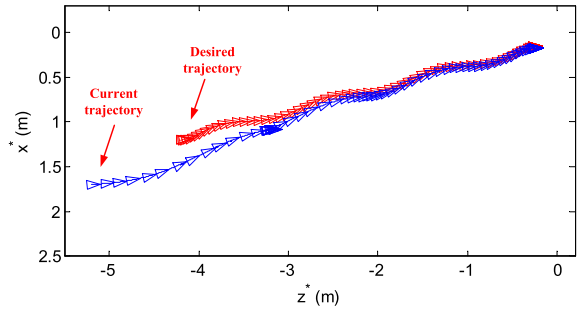

FIGURE 3. The proposed scheme: the mobile robot motion trajectory, with desired and current motion trajectories marked.

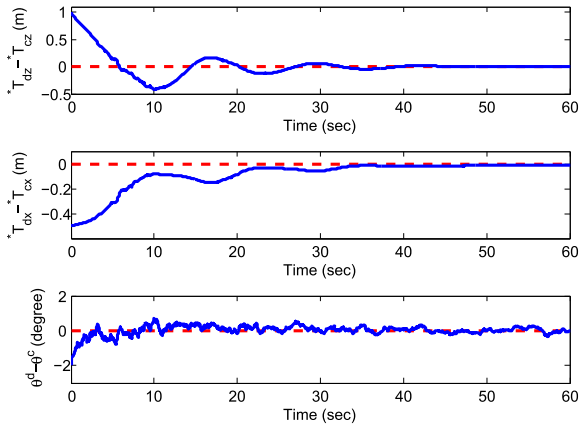

FIGURE 4. The proposed scheme: evolution of tracking errors of the mobile robot [dashed lines: desired values (zero)].

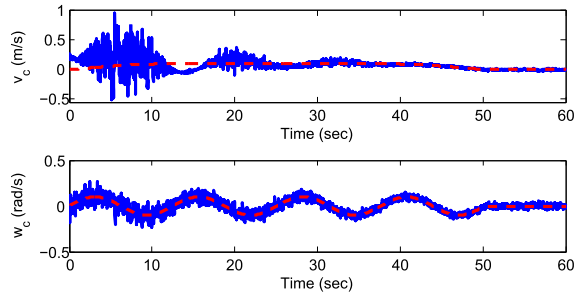

FIGURE 5. The proposed scheme: velocities of the mobile robot [solid lines: current velocities; dashed lines: velocities of the target trajectory].

system is steered by sinusoidal style velocities. Moreover, the provided scheme is compared with the classical visual servo tracking strategy in [27] and the unified visual servoing method in [31].

Moreover, to realize the designed control scheme, the system error measurement, parameter updating, and control law are executed in sequential programs. Thus, the rate of updating $\hat{\alpha}(t)$ is coincident with that of measurable input signals $\rho_1(t)$, $\rho_2(t)$, $\rho_3(t)$, $\bar{v}_d(t)$, $w_c(t)$.

The desired trajectory is set starting from pose $(-4.2\text{m}, 1.2\text{m}, 3°)$, then it moves in snake style. The current

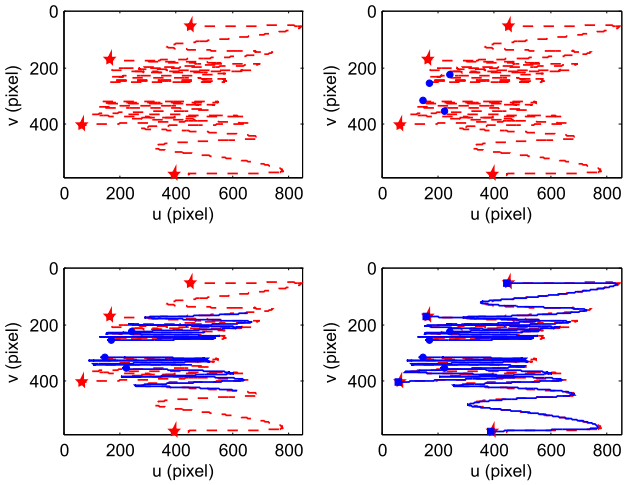

FIGURE 6. The proposed scheme: image trajectories of the features (from top left to bottom right: evolution of current and desired image trajectories) [dashed and solid lines: desired and current image trajectories, respectively; star points: final image of the desired trajectory; circular points: initial image of the current trajectory; square points: final image of the current trajectory].

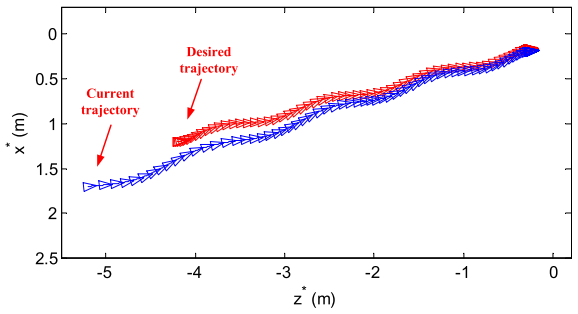

FIGURE 7. The strategy in [27]: the mobile robot motion trajectories, with desired and current motion trajectories marked.

motion trajectory is set starting from $(-5.2\text{m}, 1.7\text{m}, 5°)$. Gaussian noises are added on both desired images sequence and the current image with standard deviation $\delta = 0.2$ pixels.

For the proposed scheme, the control parameters are chosen as $k_v = 0.3, k_w = 0.3, \Gamma = 80$. Moreover, the filtered backward differential algorithm is utilized to calculate desired velocities $\bar{v}_d(t), w_d(t)$. Fig. 3 presents both the current and desired trajectories of the robot. Fig. 4 shows tracking errors of the robot between the desired and current motion trajectories, where ${}^*T_{dz}(t), {}^*T_{dx}(t)$ represent z, x coordinates of frame $\mathcal{F}^d$ origin under $\mathcal{F}^*$, and ${}^*T_{cz}(t), {}^*T_{cx}(t)$ represent z, x coordinates of frame $\mathcal{F}^c$ origin under $\mathcal{F}^*$. According to Fig. 3 and Fig. 4, we know that the mobile robot reaches the desired motion trajectory rapidly though initial errors are relatively large. Fig. 5 displays linear and angular velocities of the robot, we see that the current velocities are coincident with the desired ones as the mobile robot moves. Fig. 6 shows the image trajectories, where we see that the current features are conformed well with the desired images sequence.

The control parameters k_v, k_w, γ_1 of the compared method [27] are chosen as $k_v = 0.3, k_w = 0.1, \gamma_1 = 8$ after carefully tuning, and its results are shown in Figs. 7−10. The motion trajectories and the pose errors are shown in Figs. 7 and 8, respectively. Figs. 9 and 10 shows the velocities of the robot and the image trajectories, respectively. For the trajectories configuration, the longitudinal and lateral tracking errors are 1.0m and 0.6m at the initial time, respectively, which are quite large to be tracked. Nevertheless, the tracking errors are quickly reduced in 10 seconds after the proposed controller works, and the errors are suppressed sufficiently small in about 22 seconds. For the compared method, the lateral error is sufficiently small after about 35 seconds, and the orientation error converge after 50 seconds. Thus, it is known that the tracking errors converge slowly by the compared controller [27]. By comparing Figs. 3−6 with Figs. 7−10, we know that, with the same desired motion trajectory and target features, the response of the proposed strategy is superior over that of the method [27], in the sense that the trajectory tracking errors converge to zero more rapidly.

For the compared method [31], the control parameters are tuned as $\gamma_1 = 2, \gamma_2 = 0.5, \gamma_3 = 0.1, k_1 = 0.4, k_2 = 5, \Gamma_1 = 100, \Gamma_2 = 100$, and the results are shown in Fig. 11−12. We see that the tracking errors converge quickly in about 15 seconds. However, the chattering phenomenon occurs for the angular velocity when the tracking errors are large, though the angular velocity is filtered. Comparing with [31], the proposed method utilize moderate linear and angular velocities to obtain the comparable tracking performance. Moreover, 7 control parameters

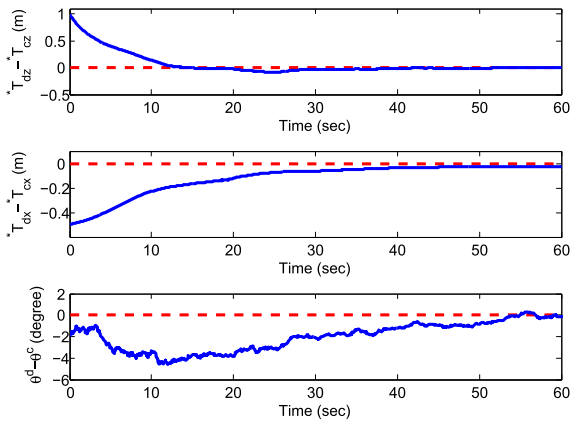

FIGURE 8. The strategy in [27]: evolution of tracking errors of the mobile robot [dashed lines: desired values (zero)].

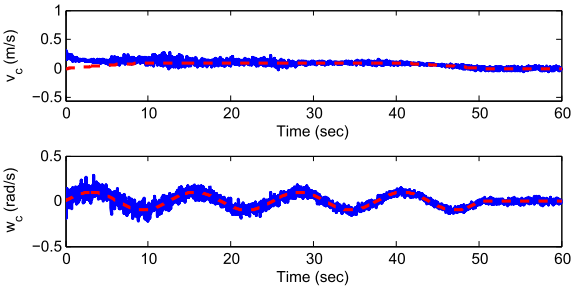

FIGURE 9. The strategy in [27]: velocities of the mobile robot [solid lines: current velocities; dashed lines: velocities on the desired trajectory].

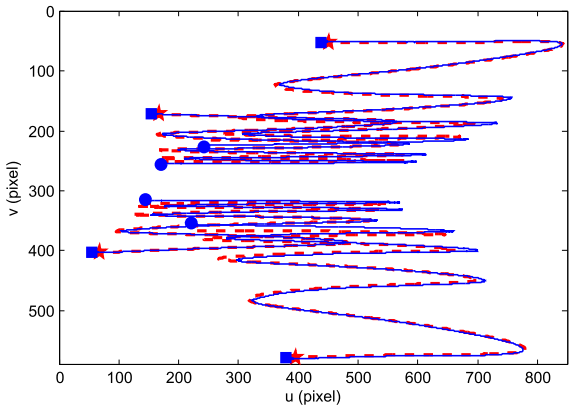

FIGURE 10. The strategy in [27]: 2D trajectories of feature points in the image space [solid line: current image trajectories; dashed line: desired image trajectories].

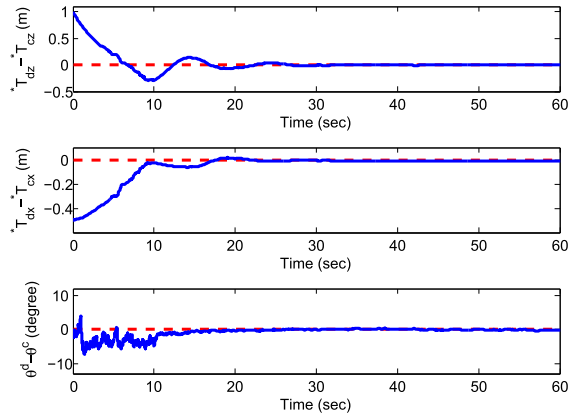

FIGURE 11. The strategy in [31]: evolution of position and orientation errors of the mobile robot poses [dashed line: desired values (zero)].

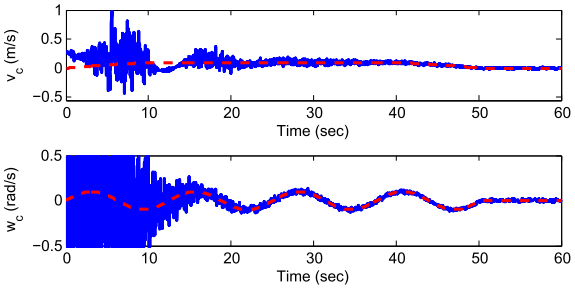

FIGURE 12. The strategy in [31]: linear and angular velocities for the mobile robot [solid line: current velocities; dashed line: velocities on the desired trajectory].

should be tuned carefully to obtain satisfied tracking performance in the method [31], and the proposed method only need 3 parameters to be tuned. Thus, the proposed scheme is more appropriate for practical use than [31] in the tracking task.

It should be noted that, in the simulation scenario, both $v_d(t)$ and $w_d(t)$ are set to zero at the last of the sinusoidal desired velocities. Although the theoretical analysis is established provided that $v_d(t)$ should not equal to zero for infinite time, it is seen that the proposed controller have a good performance when the desired linear velocity keeps zero at the last of the desired trajectory, illustrating that this method is appropriate for practical use.

V. CONCLUSIONS

For a wheeled mobile robot carrying an onboard vision system, a visual servo trajectory tracking scheme is provided in the paper. In this method, a 2-1/2-D composite tracking errors are constructed by image features and relevant poses orientation firstly. Then, the open-loop system dynamics is obtained after introducing a new error signal set. Subsequently, based on Lyapunov techniques, an adaptive kinematic controller is developed to maneuver the mobile robot tracking a given motion trajectory, with the unknown feature depth compensated by an online updating mechanism. Comparative simulations results are collected to validate the provided method. In the future efforts, we will take into account the situations that intrinsic parameters of the camera are unknown as well as camera external parameters exist and are unknown, which can make the vision-based mobile robot systems be applied to practices more conveniently.

REFERENCES

[1] Y.-L. Kuo, B.-H. Liu, and C.-Y. Wu, "Pose determination of a robot manipulator based on monocular vision," *IEEE Access*, vol. 4, pp. 8454–8464, Nov. 2016.

[2] Y. Fang, W. E. Dixon, D. M. Dawson, and P. Chawda, "Homography-based visual servo regulation of mobile robots," *IEEE Trans. Syst., Man, Cybern. B, Cybern.*, vol. 35, no. 5, pp. 1041–1050, Oct. 2005.

[3] G. Hu, W. P. Tay, and Y. Wen, "Cloud robotics: Architecture, challenges and applications," *IEEE Netw.*, vol. 26, no. 3, pp. 21–28, May 2012.

[4] D. G. K. Madusanka, R. A. R. C. Gopura, Y. W. R. Amarasinghe, and G. K. I. Mann, "Hybrid vision based reach-to-grasp task planning method for trans-humeral prostheses," *IEEE Access*, vol. 5, pp. 16149–16161, Jul. 2017.

[5] R. T. Fomena, O. Tahri, and F. Chaumette, "Distance-based and orientation-based visual servoing from three points," *IEEE Trans. Robot.*, vol. 27, no. 2, pp. 256–267, Apr. 2011.

[6] A. P. Dani, N. R. Fischer, and W. E. Dixon, "Single camera structure and motion," *IEEE Trans. Autom. Control*, vol. 57, no. 1, pp. 241–246, Jan. 2012.

[7] G. Lopez-Nicolas, N. R. Gans, S. Bhattacharya, C. Sagues, J. J. Guerrero, and S. Hutchinson, "Homography-based control scheme for mobile robots with nonholonomic and field-of-view constraints," *IEEE Trans. Syst. Man, Cybern. B, Cybern.*, vol. 40, no. 4, pp. 1115–1127, Aug. 2010.

[8] X. Liang, H. Wang, Y.-H. Liu, T. Liu, and W. Chen, "Formation control of nonholonomic mobile robots without position and velocity measurements," *IEEE Trans. Robot.*, vol. 34, no. 2, pp. 434–446, Apr. 2018.

[9] H. Chen, C. Wang, Z. Liang, D. Zhang, and H. Zhang, "Robust practical stabilization of nonholonomic mobile robots based on visual servoing feedback with inputs saturation," *Asian J. Control*, vol. 16, no. 3, pp. 692–702, 2014.

[10] J. Liao, Z. Chen, and B. Yao, "Performance-oriented coordinated adaptive robust control for four-wheel independently driven skid steer mobile robot," *IEEE Access*, vol. 5, pp. 19048–19057, Oct. 2017.

[11] H. Wang, B. Yang, J. Wang, W. Chen, X. Liang, and Y.-H. Liu, "Adaptive visual servoing of contour features," *IEEE/ASME Trans. Mechatronics*, vol. 23, no. 2, pp. 811–822, Apr. 2018.

[12] R. Brockett, "The early days of geometric nonlinear control," *Automatica*, vol. 50, no. 9, pp. 2203–2224, Sep. 2014.

[13] G. Hu, N. Gans, N. Fitz-Coy, and W. Dixon, "Adaptive homography-based visual servo tracking control via a quaternion formulation," *IEEE Trans. Control Syst. Technol.*, vol. 18, no. 1, pp. 128–135, Jan. 2010.

[14] H. Wang, C. Wang, W. Chen, X. Liang, and Y. Liu, "Three-dimensional dynamics for cable-driven soft manipulator," *IEEE/ASME Trans. Mechatronics*, vol. 22, no. 1, pp. 18–28, Feb. 2017.

[15] S. Blazic, "On periodic control laws for mobile robots," *IEEE Trans. Ind. Electron.*, vol. 61, no. 7, pp. 3660–3670, Jul. 2014.

[16] D. Chwa, "Sliding-mode tracking control of nonholonomic wheeled mobile robots in polar coordinates," *IEEE Trans. Control Syst. Technol.*, vol. 12, no. 4, pp. 637–644, Jul. 2004.

[17] Z. Li, J. Deng, R. Lu, Y. Xu, J. Bai, and C.-Y. Su, "Trajectory-tracking control of mobile robot systems incorporating neural-dynamic optimized model predictive approach," *IEEE Trans. Syst., Man, Cybern., Syst.*, vol. 46, no. 6, pp. 740–749, Jun. 2016.

[18] M. Zambelli, Y. Karayiannidis, and D. V. Dimarogonas, "Posture regulation for unicycle-like robots with prescribed performance guarantees," *IET Control Theory Appl.*, vol. 9, no. 2, pp. 192–202, Jan. 2015.

[19] Y. Wang, H. Lang, and C. W. D. Silva, "A hybrid visual servo controller for robust grasping by wheeled mobile robots," *IEEE/ASME Trans. Mechatronics*, vol. 15, no. 5, pp. 757–769, Oct. 2010.

[20] Y. Fang, X. Liu, and X. Zhang, "Adaptive active visual servoing of nonholonomic mobile robots," *IEEE Trans. Ind. Electron.*, vol. 59, no. 1, pp. 486–497, Jan. 2012.

[21] G. L. Mariottini and D. Prattichizzo, "Image-based visual servoing with central catadioptric cameras," *Int. J. Robot. Res.*, vol. 27, no. 1, pp. 41–56, Jan. 2008.

[22] X. Zhang, Y. Fang, and N. Sun, "Visual servoing of mobile robots for posture stabilization: From theory to experiments," *Int. J. Robust Nonlinear Control*, vol. 25, no. 1, pp. 1–15, 2015.

[23] K. Wang, Y. Liu, and L. Li, "Visual servoing trajectory tracking of nonholonomic mobile robots without direct position measurement," *IEEE Trans. Robot.*, vol. 30, no. 4, pp. 1026–1035, Aug. 2014.

[24] F. Yang, C. Wang, and G. Jing, "Adaptive tracking control for dynamic nonholonomic mobile robots with uncalibrated visual parameters," *Int. J. Adap. Control Signal Process.*, vol. 27, no. 8, pp. 688–700, 2013.

[25] W. E. Dixon, D. M. Dawson, E. Zergeroglu, and A. Behal, "Adaptive tracking control of a wheeled mobile robot via an uncalibrated camera system," *IEEE Trans. Syst., Man, Cybern. B, Cybern.*, vol. 31, no. 3, pp. 341–352, Jun. 2001.

[26] X. Liang, H. Wang, W. Chen, D. Guo, and T. Liu, "Adaptive image-based trajectory tracking control of wheeled mobile robots with an uncalibrated fixed camera," *IEEE Trans. Control Syst. Technol.*, vol. 23, no. 6, pp. 2266–2282, Nov. 2015.

[27] J. Chen, W. E. Dixon, D. M. Dawson, and M. McIntyre, "Homography-based visual servo tracking control of a wheeled mobile robot," *IEEE Trans. Robot.*, vol. 22, no. 2, pp. 406–415, Apr. 2006.

[28] B. Jia, J. Chen, and K. Zhang, "Adaptive visual trajectory tracking of nonholonomic mobile robots based on trifocal tensor," in *Proc. IEEE/RSJ Int. Conf. Intell. Robot. Syst.*, Hamburg, Germany, Sep. 2015, pp. 3695–3700.

[29] A. Cherubini and F. Chaumette, "Visual navigation of a mobile robot with laser-based collision avoidance," *Int. J. Robot. Res.*, vol. 32, no. 2, pp. 189–205, Feb. 2013.

[30] H. M. Becerra, C. Sagüés, Y. Mezouar, and J.-B. Hayet, "Visual navigation of wheeled mobile robots using direct feedback of a geometric constraint," *Auto. Robots*, vol. 37, no. 2, pp. 137–156, Feb. 2014.

[31] B. Li, Y. Fang, G. Hu, and X. Zhang, "Model-free unified tracking and regulation visual servoing of wheeled mobile robots," *IEEE Trans. Control Syst. Technol.*, vol. 24, no. 4, pp. 1328–1339, Jul. 2016.

[32] R. Hartley and A. Zisserman, *Multiple View Geometry in Computer Vision*, 2nd ed. Cambridge, U.K.: Cambridge Univ. Press, 2003.

[33] J. J. Slotine and W. Li, *Applied Nonlinear Control*. Englewood Cliff, NJ, USA: Prentice-Hall, 1991.

FANLEI YAN received the B.Eng. degree from Yantai University, China, in 1999, the M.E. degree from Guangxi University, China, in 2004, and the Ph.D. degree in textile engineering from Tianjin Polytechnic University, Tianjin, China, in 2016.

He is currently an Assistant Professor with Tianjin Polytechnic University. His research interests include visual servoing, mobile robots, and unmanned aerial vehicle mission planning.

BAOQUAN LI (S'14–M'16) received the B.Eng. degree in automation and the Ph.D. degree in control theory and control engineering from Nankai University, Tianjin, China, in 2010 and 2015, respectively. From 2013 to 2014, he was a joint Ph.D. Student with Nanyang Technological University, Singapore, awarded by the China Scholarship Council.

He is currently an Assistant Professor with the School of Electrical Engineering and Automation, Tianjin Polytechnic University, Tianjin. His research interests include computer vision, visual servoing, and mobile robots.

WUXI SHI received the B.S. degree in mathematics from Beijing Normal University, Beijing, China, in 1989, and the M.S. and Ph.D. degrees in control theory and control engineering from Beihang University, Beijing, in 1999 and 2003, respectively.

He is currently a Professor with the School of Electrical Engineering and Automation, Tianjin Polytechnic University, Tianjin, China. His current research interests include fuzzy control theory and fuzzy predictive control.

DONGWEI WANG received the B.Eng. degree from Tianjin Polytechnic University, Tianjin, in 2015.

He is currently pursuing the M.S. degree in control science and engineering with Tianjin Polytechnic University. His research interests include computer vision and mobile robots.